



Force frequency effect in square quartz crystals

M. M. Mohammadi*¹, M. Hamedi²

¹Engineering faculty, University of Zanjan, Zanjan, Iran

²Mechanical engineering faculty, University of Tehran, Tehran, Iran

ABSTRACT: In this investigation, the force-frequency effect in a square AT-Cut quartz resonator is studied. Based on the force-frequency effect, by insertion of diametrical forces, the natural frequency of thickness shear vibration mode in AT-Cut quartz resonators is changed. This criterion is of importance in designing quartz resonators and force sensors. In this paper, the frequency change of a square AT-Cut quartz crystal subjected to a pair of opposing forces on different points of its edge is studied experimentally. Also, the force-frequency effect in the square crystal is modeled by a previously developed mathematical-finite element model. The accuracy of the model is verified by the experimental results. Then, the model is applied for evaluating the force-frequency effect in the AT-Cut crystal, and the frequency shifts in different loading configurations are obtained. The new loading configurations are produced by moving the loading points along the edges, and by rotating the edges of the crystal around its thickness axis. Also, the distributed loading tests are performed on the crystal. Based on this, the loading configurations with maximum and minimum frequency shifts are obtained. Moreover, the design of quartz crystal force sensors having high sensitivity and also the crystal oscillator with high-frequency stability are discussed.

Review History:

Received: Jan. 22, 2020

Revised: Nov. 09, 2020

Accepted: Nov. 09, 2020

Available Online: Nov. 22, 2020

Keywords:

AT-Cut quartz

Force-frequency effect

Square resonator

Experimental study

Hybrid mathematical-numerical model

1- Introduction

Quartz crystal is a piezoelectric material and is widely used for the production of crystal resonators, oscillators, and sensors [1-3]. Upon the inverse piezoelectric effect, quartz crystals vibrate by the application of alternative voltage. The mode of vibration depends on the crystal cut angles. For example, an X-cut crystal exhibits an extensional vibration mode whereas the AT-Cut vibrates in the thickness shear mode. If the frequency of alternating voltage equals the natural frequency of the quartz crystal, resonance occurs. The resonance frequency of the crystal can be detected by a network analyzer or a frequency counter. When a quartz resonator is subjected to an initial mechanical biasing field, its resonance frequency changes. This Frequency Shift (FS) is related to the force-frequency effect.

The frequency stability of crystal resonators and oscillators and the sensitivity of quartz pressure and load sensors directly depend on the force-frequency effect. In 1965, Ratajski defined the force-frequency coefficient and measured the coefficient for circular singly rotated quartz crystals [4]. Ballato et al. investigated the force-frequency effect for doubly rotated quartz crystals with a circular shape. Also, they studied the effect of applied acceleration on the frequency of the crystal [5]. Valdois et al. introduced a new cut of quartz crystal, named SBCT cut, which its resonance

frequency was not affected by the applied load and mechanical stress [6].

Investigations on force-frequency effect led to the introduction of quartz resonator force and pressure sensors with high sensitivity and small sizes, and also crystal resonators with higher frequency stability. However, the quartz crystal in most of these sensors and resonators has a circular shape, and the force-frequency coefficient has been introduced for circular quartz disc [7-10]. Some researchers have used non-circular quartz crystals as the resonating element. For example, Murozaki et al. designed a highly sensitive, wide-measurement-range compact load sensor using micro-fabrication technology. The resonating member of the sensor was a square quartz resonator, and distributed load has been applied on one of its edges. Also, this research team designed a three-layer quartz resonator load sensor for detecting bio-signals with a wide measurement range. They used a square quartz resonating member in their design [11]. Murozaki et al. made a wide range load sensor using vacuum-sealed square quartz crystal resonators for measuring bio-signals on the bed. Their sensing system could detect the body weight, heartbeat, and respiration simultaneously by just lying on the bed [12]. Arai et al. developed a wide range load sensor using rectangular quartz resonators. The resonating quartz plate was sandwiched between a pair of holding layers. The holding layers restrained the quartz plate from buckling during the load measurements [13].

*Corresponding author's email: dr.mohammadi@znu.ac.ir



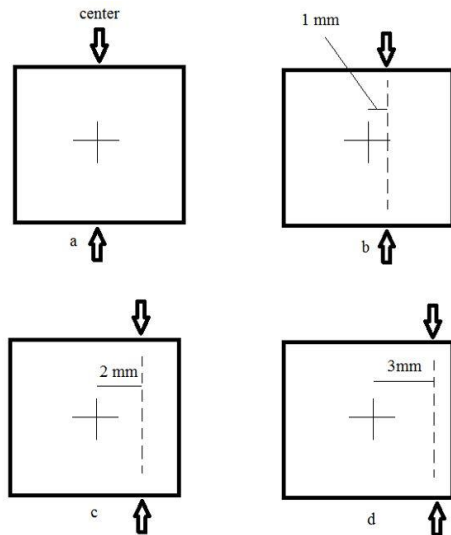


Fig. 1. Loading configurations of the crystal at force-frequency experiment



Fig. 2. Loading fixture for performing force-frequency experiments

A survey of the literature shows that the force-frequency effect for the circular resonators has been extensively studied [14-16]. However, this effect has not been investigated for the square resonators. On the other hand, a growing body of literature has focused on the application of square resonators in load sensors. Therefore, analyzing the force-frequency effect for square resonators is necessary. In this article, we evaluate the force-frequency effect for the square resonators. For this, some force-frequency experiments are performed and a previously developed hybrid analytical-Finite Element Method (FEM) model is employed for analyzing the force-frequency effect in this type of quartz resonator [17, 18]. Also, the design of the load sensors with higher sensitivities and resonators with higher frequency stabilities are discussed.

In the first part of the paper (sections 2-4), some force-frequency experiments are performed on a square AT-Cut quartz crystal, and the results are used for the validation of the numerical-mathematical model. In the second part, the hybrid model is applied for a complete analysis of the force-frequency effect on the aforementioned square quartz crystal.

2- Force-Frequency Experiments on a Square Quartz Resonator

As the first step of this investigation, the force-frequency experiments have been performed by applying opposing forces to the edge of a crystal and parallel with “Z” or X_3 crystallographic axis. For this, an 8 mm length AT-Cut quartz square was subjected to a pair of opposing forces on its edges. The resonator had a thickness of 0.46 mm with the series thickness-shear resonance frequency of 3.578545 MHz. There are four loading configurations with different locations of loading points along the edge of the crystal. Fig.

1 represents the loading configurations.

A special fixture was constructed for loading the crystals. Fig. 2 represents the loading fixture. In this figure, piece (1) is the loading weight, pieces (2 and 3) are upper and lower anvils, respectively, and piece (4) is the square quartz crystal. The square quartz crystal was positioned between the upper and lower anvils and the loading was performed by putting standard weights on the upper anvil of the fixture.

Our measurement system involves a signal generator with a resolution of 0.1 Hz, and an oscilloscope with a resolution of 1 Hz. The system is represented in Fig. 3. The loading fixture was placed in an electric oven. In this article, the results of force-frequency experiments which were performed at room temperature were reported. A simple circuit, including the crystal and connecting wires and a resistor, is used in measurements. When the frequency of the output signal of the signal generator becomes close to the natural frequency of thickness-shear vibration mode of the crystal, the resonance occurs. At the resonance state, the crystal resonator serves as a pure resistor. Thus, the output signal of the signal generator can be seen at an oscilloscope without amplitude and phase shift. If the frequency of the signal generator is far from the resonance frequency, the amplitude of the output signal observed in the oscilloscope will be smaller than the input signal [19].

The applied loads were 0.9 and 1.8 N, and the experiments were performed 5 times for each loading configuration. Table 1 represents the average experimental FS's for each loading configuration.

As seen in Table 1, the FS's depend on the position of loading points and the amount of applied force. Also, by moving the loading point from the center to the corner of the



Fig. 3. Measuring the crystal frequency by a signal generator and an oscilloscope

Table 1. FS of the crystal for different loading configurations (Hz)

configuration	force			
	a	b	c	d
0.9 N	-15	-12	2	13
1.8 N	-25	-20	3	23

crystal, the sign of FS has changed.

3- Hybrid Mathematical-FEM Model of Force-Frequency Effect

The hybrid mathematical- FEM model concludes two distinct parts: The mathematical part which calculates the FS's and the FEM part which calculates stress components, and these components are fed to the mathematical part of the model.

In our previous work [18], we extracted two-dimensional equations for high-frequency vibrations of crystal plates under initial mechanical stresses and homogeneous thermal strains, using Mindlin Procedure [20]. These equations were applied for thickness shear vibrations of rotated Y-Cut quartz crystals. We derived an analytical equation for calculating the change of fundamental thickness-shear frequencies in terms of initial thermal and mechanical strains, and second and third-order elastic constants, for rotated Y-Cut quartz crystals.

Then, the equation was validated for AT-Cut quartz crystals. The equation is:

$$\left(\frac{\Delta f}{f_0}\right)_m = (U_{1,1}^{(0)})_m + \frac{1}{2C_{66}^\theta} [C_{661}^\theta (E_1^{(0)})_m + C_{662}^\theta (E_2^{(0)})_m + C_{663}^\theta (E_3^{(0)})_m + C_{664}^\theta (E_4^{(0)})_m] \quad (1)$$

where $(\Delta f / f_0)_m$, $(E_i^{(0)})_m$ and $(U_{1,1}^{(0)})_m$ are the frequency shift, zero-order mechanical strain, and displacement gradient which are induced upon the application of mechanical strains. Also, C_{66}^θ and C_{66i}^θ are second and third-order elastic constants of quartz at temperature θ . Here θ is the room temperature and all the material constants are available at room temperature [3]. For convenience, the abbreviated

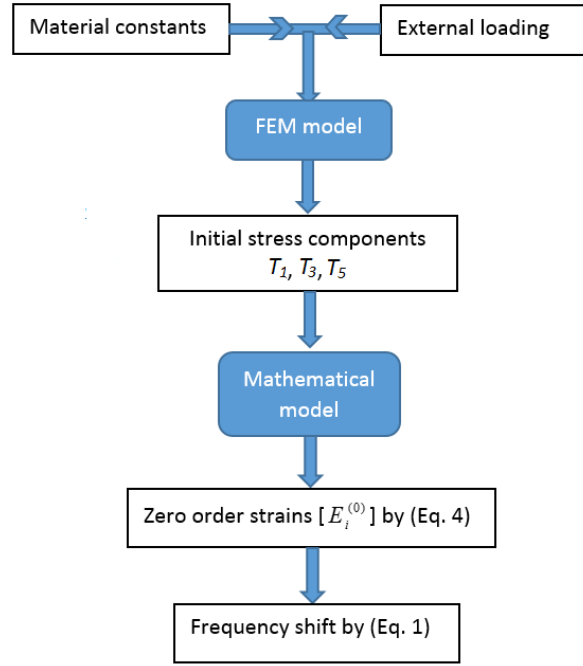


Fig. 4. The algorithm for hybrid FE-mathematical modeling of force-frequency effect

(Voigt) notation has been employed in Eq. (1). It should be noted that this mathematical model produces similar results to the model proposed by Lee at room temperature [21].

Considering the anisotropic properties of quartz is vital for accurate modeling of the force-frequency effect. However, piezoelectricity can be neglected. Thus, the body was considered to be anisotropic and the initial displacements, strains, and stresses include the effects of external tractions and do not include any piezoelectric effect [17].

For calculating the strain components in Eq. (1), we used the finite element method. In our model, the standard linear Lagrangian formulation from the theory of elasticity is applied to solve for the initial stress and strains. These equations are:

$$\begin{aligned}
 T_{ij} &= \frac{1}{2} C_{ijkl} (U_{k,l} + U_{l,k}), \\
 T_{ij,j} &= 0 \quad \text{in } V \\
 P_i &= N_j T_{ij} \quad \text{on } S
 \end{aligned} \tag{2}$$

where T_{ij} and $U_{i,j}$ are the second Piola-Kirchhoff stress tensor and the initial displacement gradient, P_i is the surface traction in the boundary surfaces, C_{ijkl} are the fourth-order stiffness coefficients and N_j is a surface normal vector. Neglecting higher-order Mindlin strain terms, zero-order strain in Eq. (1) may be obtained by [18]:

$$E_{ij}^{(0)} = S_{ijkl} T_{kl} \tag{3}$$

where S_{ijkl} are the compliance coefficients of AT-Cut quartz. For AT-Cut crystal, Eq. (3) may be written in the following form, using Voigt notation [17, 18]:

$$\begin{aligned}
 E_1^{(0)} &= S_{11} T_1 + S_{13} T_3 + S_{15} T_5, \\
 E_2^{(0)} &= S_{21} T_1 + S_{23} T_3 + S_{25} T_5, \\
 E_3^{(0)} &= S_{31} T_1 + S_{33} T_3 + S_{35} T_5, \\
 E_4 &= S_{41} T_1 + S_{43} T_3 + S_{45} T_5.
 \end{aligned} \tag{4}$$

4- Calculation of Initial Stress Components by FEM

Eq. (2) contains the governing equations for finite element analysis of initial stresses in square AT-Cut quartz resonator. By calculating the stress components T_1 , T_3 and T_5 in the center of the loaded square quartz resonators via FEM and substituting these values into Eq. (4), zero-order strain components are obtained. By substituting the zero-order strain components into Eq. (1) frequency shift of the crystal is determined. The modeling procedure is laid out in Fig. 4.

The stress components were obtained for an 8 mm length plano-convex square AT-Cut quartz resonator which was subjected to a pair of opposing forces on its edges. The material was supposed to be linear elastic and the

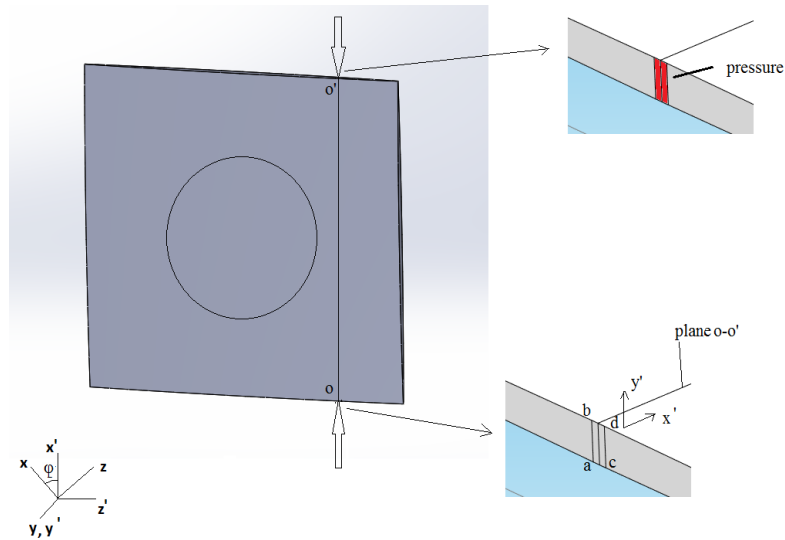


Fig. 5. Loading of the crystal and the boundary conditions in FEM in an arbitrary loading configuration

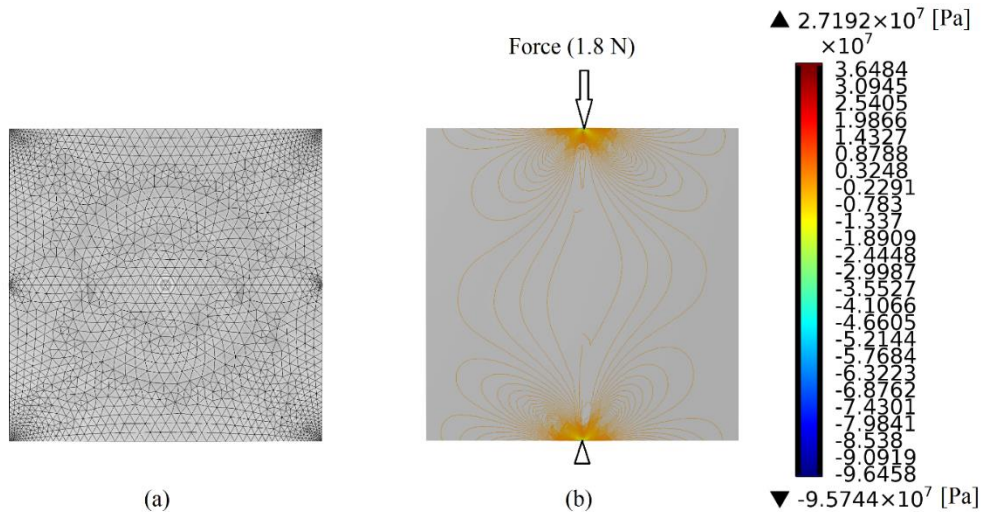


Fig. 6. (a) Meshed geometry of the square resonator, (b) Second Piola-Kirchhoff stress component T_1

anisotropy of the material was taken into account. Second-order elastic constants of AT-Cut quartz were introduced to the finite element model. These coefficients were reported in appendix (A). The simulations were performed using the solid mechanics module in COMSOL software.

By applying a pair of opposing forces with the magnitude of 0.9 and 1.8 N, on different points of the upper and lower edges of the resonator, the initial stress components are obtained in the crystal. For applying the forces in simulations, small contact areas were defined on the crystal edge. The width of the rectangular contact areas was 0.1 mm and their length was equal to the crystal thickness on the loading point. Then, a unique pressure was applied to the contact area. The magnitude of the applied pressure was adjusted based on the opposing forces. Fig. 5 shows the loading of

the crystal and the boundary conditions in the simulations. For defining the boundary conditions, a rotated coordinate system (x', y', z') was defined by rotating the x or z axis of the crystal by angle φ . The plane $o-o'$ has no movement in z' direction. The surface $(abcd)$ in Fig. 5 has no movement in x' direction, also the line “bd” or the line “ac” has no movement in y directions. These boundary conditions were selected in accordance with the experiments and led to the convergence of finite element results.

Fig. 6 (a) shows the meshed geometry of the loaded resonator at one of the loading configurations. The FE model has 17478 tetrahedral elements. The second Piola-Kirchhoff stress tensor component T_1 was reported at part b of Fig. 6.

For ensuring the accuracy of the FE-model, the mesh dependency analysis was performed and the three stress

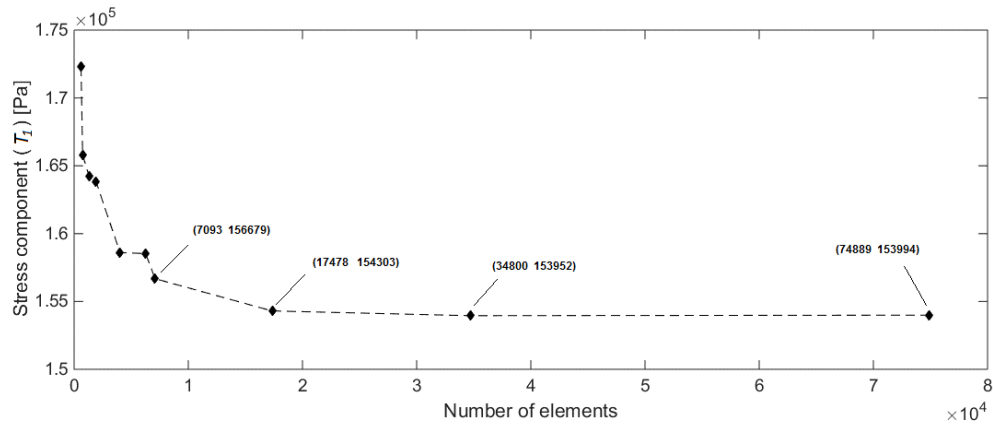


Fig. 7. Variation of stress component (T1) with the number of elements

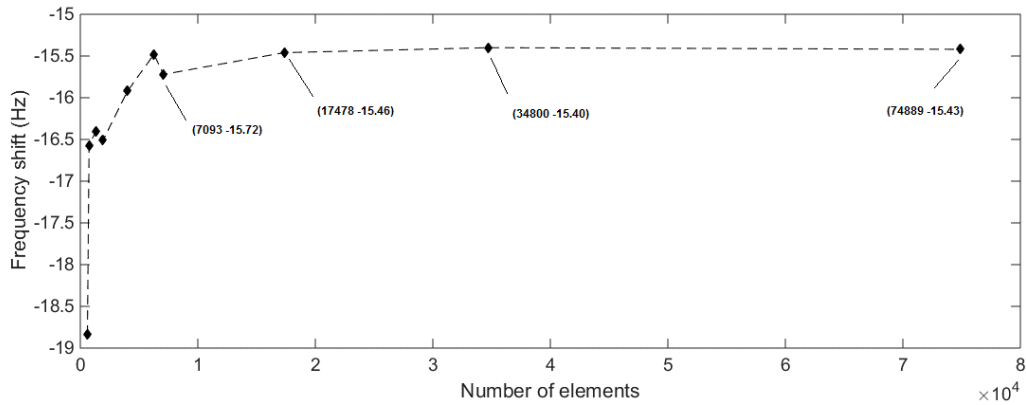


Fig. 8. Dependence of frequency shift to the number of elements

components (T_1 , T_3 , T_5) in loading configuration (a) were calculated. For instance, the variation of stress component T_1 and the calculated frequency shifts for loading configuration (a) with the applied load of (0.9 N) were represented in Fig. 7. As shown in Fig. 7, when the number of elements varies between 17478 and 74889 the stress component T_1 changes from 154303 Pa to 153994 Pa and the error is almost 0.2%.

By using the three stress components (T_1 , T_3 , T_5) and calculating the zero-order strain components using Eq. (4) and substituting them into Eq. (1), the frequency shift was calculated as a function of the number of elements. Fig. 8 shows the dependence of frequency shift to the number of elements. It is evident that by increasing the number of elements from 17478 to 74889 the frequency shift varies from -15.46 to -15.43 and the frequency error is 0.03 Hz which is acceptable for the model. Thus, our finite element simulations were performed with 17478 elements.

By performing the finite element analysis for all the loading configurations, the second Piola-Kirchhoff stresses (T_1 , T_3 and T_5) were determined at the center of the resonator and substituted at Eq. (4) for calculating the zero-order strain

components. These strain components were substituted into Eq. (1) to calculate for the FS's. Fig. 9 represents the modeled and experimental FS's for the four loading configurations with two different concentrated forces.

As seen in Fig. 9, there is good accordance between the model and experimental results. The average frequency difference between the model results and the experiments for 1.8 N and 0.9 N loads are 7.25 Hz and 4 Hz respectively. Also, both the model and experiments demonstrate the variation of FS and change in the sign of FS, by moving the loading point from the center of the rim (loading configuration a) to its corner (configuration b). According to the model results, the FS becomes zero at a 2.3 mm distance from the center of the edge. This distance decreases to almost 1.9 mm for the experiments. Upon the mathematical model, the occurrence of zero frequency shifts in some loading configurations depends on the initial stress components and the corresponding zero-order Mindlin strains i.e. $E_1^{(0)}$, $E_2^{(0)}$, $E_3^{(0)}$ and $E_4^{(0)}$. Variation of the loading states results in the variation of these four-strain components. Fig. 10 represents the variation of zero-order Mindlin strains along the crystal edge (part a), and

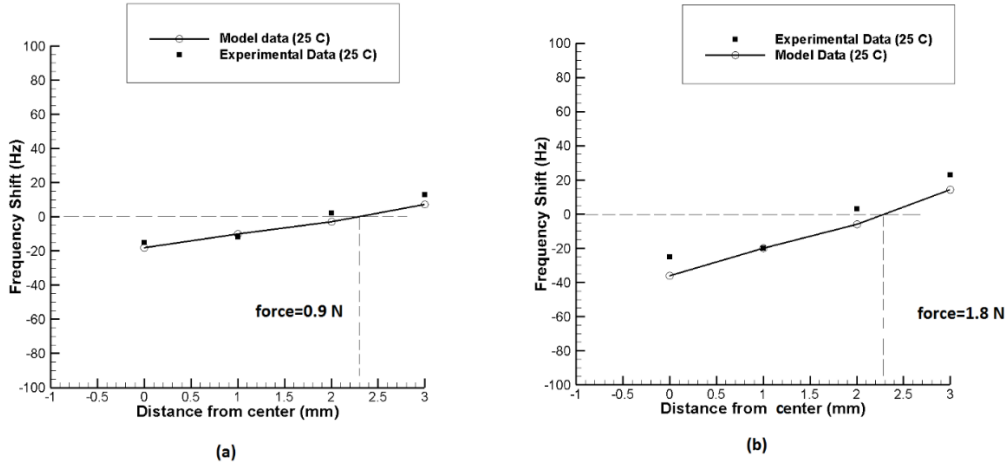


Fig. 9. The Experimental and modeled FS's at four loading configurations (a) 0.9 N loading (b) 1.8 N loading

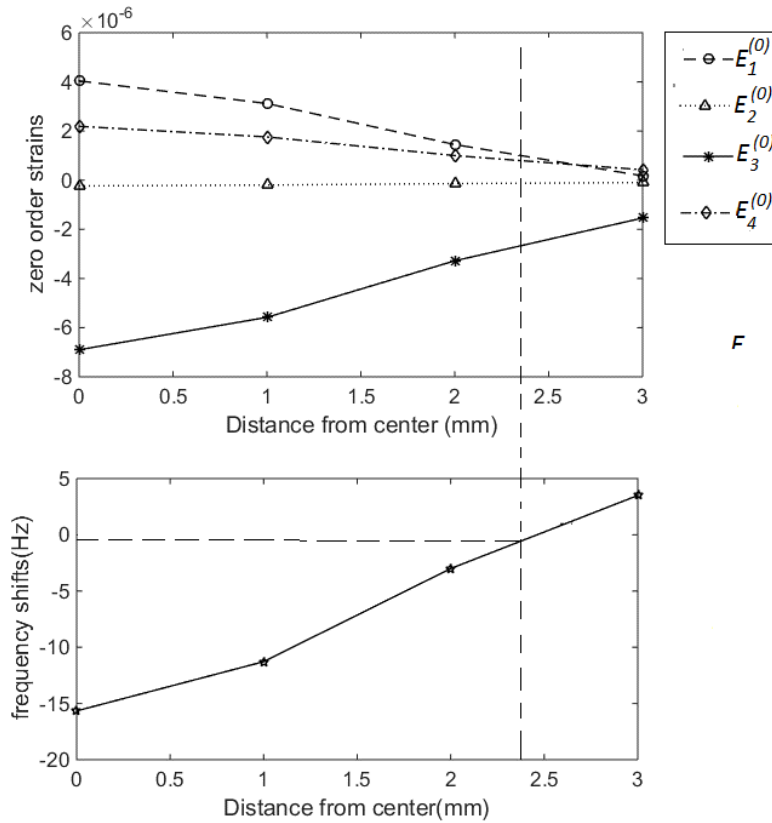


Fig. 10. strain components vs. frequency shift for the experiments (force=0.9N)

the corresponding frequency shift (part b). As shown by Fig. 10, in the zero frequency shift point, the strain components $E_1^{(0)}$, $E_2^{(0)}$ and $E_3^{(0)}$ are effective and the strain component $E_3^{(0)}$ compensates for the effect of the other two strain components. For instance, when the applied force is 0.9 N, the point at which zero frequency shift occurs, is 2.3 mm distance from the center point of the crystal edge. In this point, using Eq. (1), and by neglecting the small strain component $E_4^{(0)}$

and applying $E_1^{(0)} = U_{1,1}^{(0)}$ which is true for initial fields [21], one obtains:

$$\left(1 + \frac{C_{661}^{25}}{2C_{66}^{25}}\right)E_1^{(0)} + \frac{C_{662}^{25}}{2C_{66}^{25}}E_2^{(0)} = -\frac{C_{663}^{25}}{2C_{66}^{25}}E_3^{(0)} \quad (5)$$

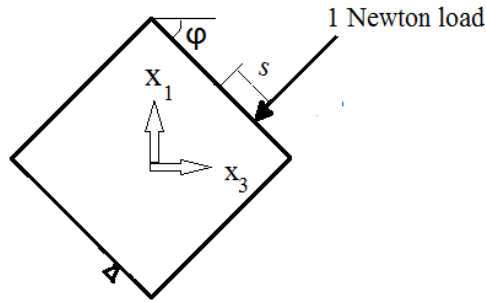


Fig. 11. Loading of the crystal with varying edge angle ϕ

Eq. (5) states the relation between zero-order strain components on the points with zero frequency shift.

The zero FS point is of importance in designing high-stability oscillators. When the resonator is used as a resonating member of an oscillator circuit, the stability of the resonance frequency is of importance. Thus lower frequency shifts make the resonator more stable to the environmental effects like accelerations and vibrations, which can introduce mechanical stresses on the resonator through the support points of the crystal. The crystal resonators in these oscillators usually are subjected to diametric forces from their supporting points due to the applied acceleration and vibration from the environment. By selecting the zero FS point as the supporting points of the crystal, the frequency instability due to the acceleration and vibration effects is reduced and the frequency stability is increased [22].

If the resonator is used as the resonating member of a load sensor, and the sensor was working based on the frequency shifts due to the insertion of the applied force, then high-frequency shift in the resonator frequency results in enhancement of the sensor sensitivity. Because the sensitivity in this application is the magnitude of frequency shifts divided by the magnitude of the force.

5- Modeling the Force-Frequency Effect for Other Loading Configurations

In the design of resonator load sensors, to enhance sensitivity, we are looking for the loading configurations with maximum FS's. For this, we employed our model for analyzing the force-frequency effect at other possible loading configurations of the square AT-Cut crystal.

5- 1- Concentrated loading of the crystal at different edge angles

By rotating the square crystal around "y" axis, other loading configurations for the crystal may be created. For the first attempt, the edge of the crystal was rotated by an angle of ϕ with respect to the axis x_3 , as shown in Fig. 11. The rotation angle, or azimuth angle, changes from 0° to 180° with the

steps of 10° .

As our previous test, by changing the loading distance "S", the loading configurations a, b, c, and d are repeated for each azimuth angle, and the FS's for each loading configuration are calculated by the proposed model. The loading distances from the central point are 0, 1, 2, and 3 mm for loading configurations a, b, c, and d respectively. The FS for each loading configuration was calculated by the abovementioned model. The calculations were performed for each 10° of azimuth angles and the results were represented in Fig. 12. As seen in Fig. 12, for loading configurations a, b, and c, there are two azimuth angles with zero FS. However, in loading configuration "d" we have not such angles. Indeed, for loading configuration "d" Eq. (5) was not satisfied. The other important data contributes to the maximum FS of the crystal for each loading configuration. Fig. 12 shows the maximum FS's and related azimuth angles. As may be seen, for all loading configurations, the maximum FS occurs at azimuth angle 90° , and the maximum FS reduces from 65 Hz at loading configuration "a" to 6.4 Hz at loading configuration "c". All the FS curves are symmetric about azimuth angle 90° . This is due to the monoclinic symmetry of AT-Cut quartz and is in accordance with the results which were reported by other researchers for circular AT-Cut resonators [4, 21].

5- 2- Distributed loading of the crystal at different edge angles

Again the crystal is rotated around its "y" axis and a uniform 0.25 N/mm distributed load is applied on its 4 mm edge. The opposing edge is laid on the lower anvil and has no movement along the normal vector of the edge. The initial stress components at the center of the crystal were calculated and fed to the mathematical model of force-frequency, as explained in previous sections. Fig. 13 represents the model results for this loading condition. As seen in Fig. 13, the maximum FS of 40.78 Hz occurs at $\phi=90^\circ$, and the zero FS's occur at $\phi=13.7^\circ$ and $\phi=167.35^\circ$. Also, the FS diagram is almost symmetric around $\phi=90^\circ$.

The highest frequency shifts occur at azimuth angle 90° , for both concentrated and distributed loading. Thus, for designing load sensors with the highest sensitivity, the azimuth angle can be 90° .

6- Conclusions

In this article, the force-frequency effect in a square AT-Cut quartz resonator was studied. Based on the results of experiments and the hybrid mathematical-FEM model, the resonance frequency of the crystal alters with the application of concentrated forces on different points of the edge of the crystal. The study was performed in three steps.

At the first step, the crystal edges were perpendicular to the AT-Cut basic axis. Four loading configurations were defined and force-FS's were obtained by the mathematical-numerical model and experiments. Results were in good accordance with each other and demonstrated the sign change of the FS by moving the loading point along the edge. Accordingly, the loading points with zero and maximum FS's were obtained.

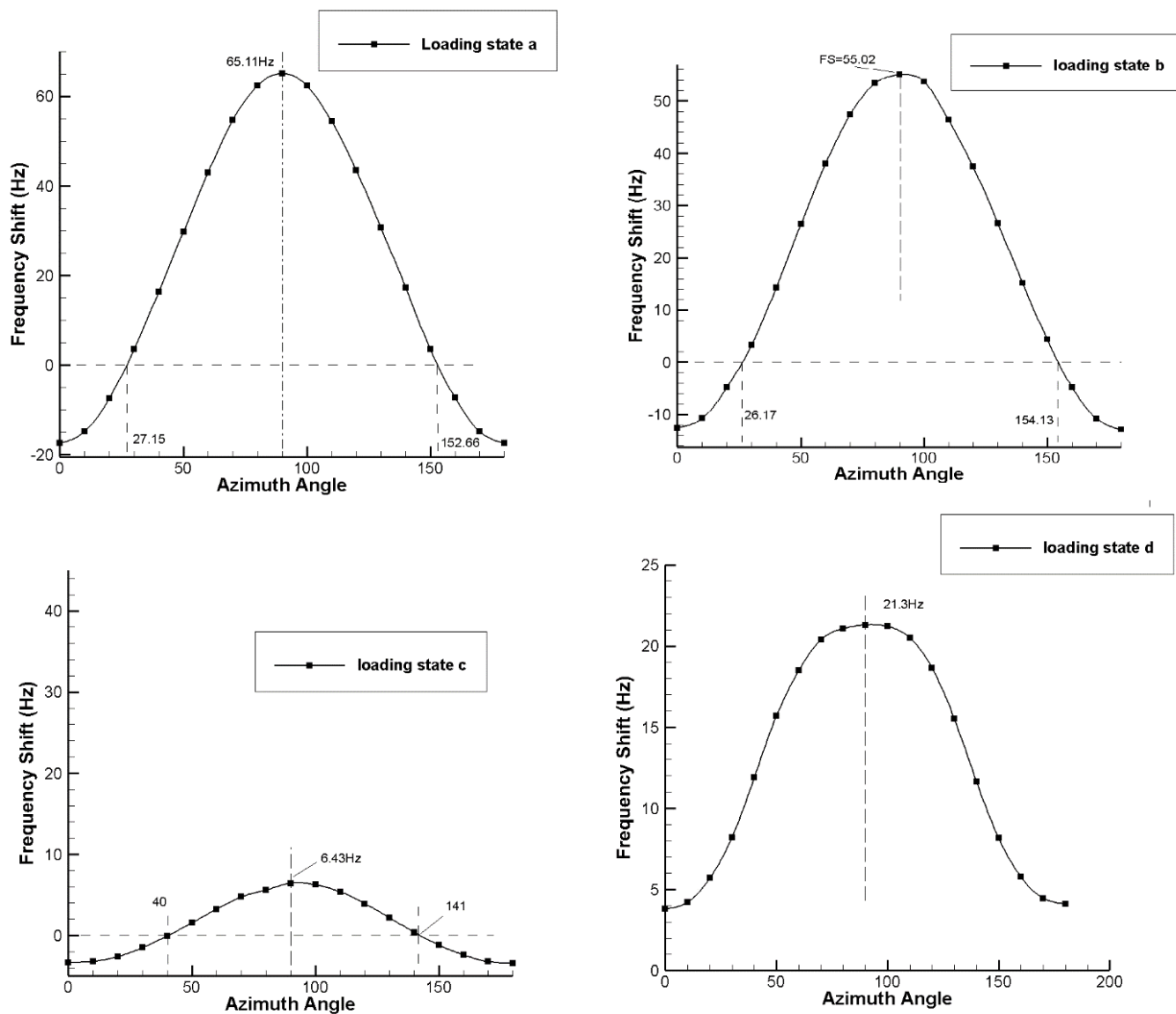


Fig. 12. The frequency shift of the crystal as a function of force azimuth angle φ at different loading configurations (a to d)

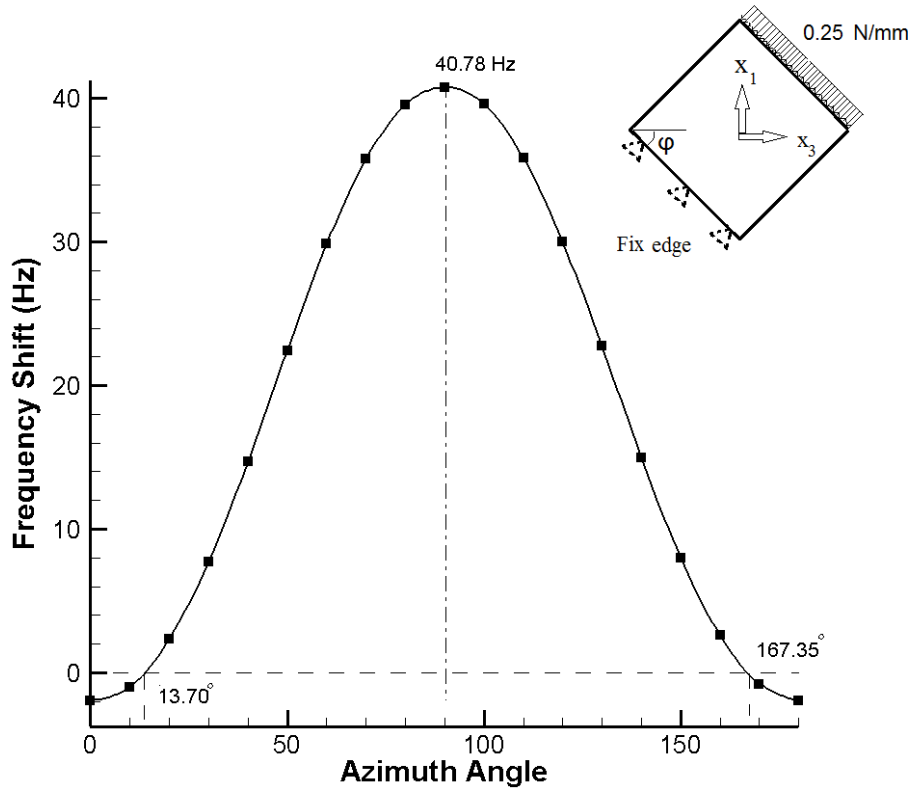


Fig. 13. The frequency shift of the crystal as a function of force azimuth angle φ for distributed loading configuration

At the second and third steps, the loading edges of the crystal were rotated around the thickness axis, and both concentrated and distributed loading tests were performed. The FS's were modeled and plotted as a function of force azimuth angle. Accordingly, the points with maximum and zero FS's, which are important in designing high sensitivity crystal load cells and ultra-stable crystal oscillators were obtained.

The results show that the most sensitive force sensor may be made by concentrated loading of the crystal at the central points of its edges with a 90° azimuth angle. Also, in almost all loading configurations, there are some points with zero frequency shifts, which are suitable for restricting the movement of crystal in oscillators and force sensors.

Nomenclature

- f_0 : Initial resonance frequency of AT-Cut resonator
- f : Thickness shear resonance frequency of resonator
- $U_{i,1}^{(0)}$: Zero order component of initial displacement gradient

- $E_r^{(0)}$: Zero order initial strains
- C_{ij} : Second order stiffness coefficient (Voigt notation)
- C_{ijk} : Third order stiffness coefficients
- T_{ij} : Initial stress components
- N_j : Surface normal vector
- $E_r^{(0)}$: Zero order initial strains
- P_i : Surface traction vector
- S_{ijkl} : Compliance tensor
- T_i : Initial stress components (Voigt notation)
- S : Concentrated loading point distance from edge center
- FS : Frequency shift

References:

[1] H. Daneshpajooh, M. Mohammadi, M. Hamed, K. Uchino, Off-Center Force Effect on Quartz Resonator Sensors, Analyzed with Nonlinear Finite Element Method, *Sensor Letters*, 16(11) (2018) 884-887.

[2] S. Pisupati, D. Kundukoori, N. Mekala, S. Kaluvan, H. Zhang, Design of resonance based DC current sensor using BAW quartz resonators, *Sensors and Actuators A: Physical*, 271 (2018) 104-110.

[3] M.S. Patel, B.K. Sinha, A dual-mode thickness-shear quartz pressure sensor for high pressure applications, *IEEE Sensors Journal*, 18(12) (2018) 4893-4901.

[4] J. Ratajski, Force-frequency coefficient of singly rotated vibrating quartz crystals, *IBM Journal of Research and Development*, 12(1) (1968) 92-99.

[5] A. Ballato, E. EerNisse, T. Lukaszek, Force-frequency effect in doubly rotated quartz resonators, Sandia Labs., Albuquerque, NM (USA), 1977.

[6] M. Valdois, B.K. Sinha, J.-J. Boy, Experimental verification of stress compensation in the SBTC-cut, *IEEE transactions on ultrasonics, ferroelectrics, and frequency control*, 36(6) (1989) 643-651.

[7] Z. Wang, Y. Dong, H. Zhu, G. Feng, Effect of transverse force on the performance of quartz resonator force sensors, *IEEE transactions on ultrasonics, ferroelectrics, and frequency control*, 51(4) (2004) 470-476.

[8] Z. Wang, H. Zhu, Y. Dong, G. Feng, Off-centre load-insensitive digital quartz resonator force sensor, *IEEE Proceedings-Science, Measurement and Technology*, 148(5) (2001) 215-220.

[9] C. Gehin, C. Barthod, Y. Teisseyre, Design and characterisation of a new force resonant sensor, *Sensors and Actuators A: Physical*, 84(1-2) (2000) 65-69.

[10] F. Chen, W. Tian, Y. Wei, Highly sensitive resonant sensor using quartz resonator cluster for inclination measurement, *Review of Scientific Instruments*, 91(5) (2020) 055005.

[11] Y. Murozaki, S. Sakuma, F. Arai, Improvement of the measurement range and temperature characteristics of a load sensor using a quartz crystal resonator with all crystal layer components, *Sensors*, 17(5) (2017) 1067.

[12] Y. Murozaki, F. Arai, Wide-range Load Sensor Using Vacuum Sealed Quartz Crystal Resonator for Simultaneous Biosignals Measurement on Bed, in: 2020 IEEE International Conference on Robotics and Automation (ICRA), IEEE, 2020, pp. 1015-1020.

[13] F. Arai, Y. Murozaki, S. Sakuma, Wide-range load sensor using quartz resonator, in, Google Patents, 2019.

[14] F. Chen, J. Gao, W. Tian, Force-frequency characteristics of multi-electrode quartz crystal resonator cluster, *Sensors and Actuators A: Physical*, 269 (2018) 427-434.

[15] W. Tian, Q. Zhao, S. Feng, B. Ma, Finite Element Analysis Of thin Quartz Wafer Stress Distribution In The Radial Force, in: 5th International Conference on Civil Engineering and Transportation, Atlantis Press, 2015.

[16] N. Goel, S. Tadigadapa, In-Situ Measurement of Stress in Thin Films using Micromachined Quartz Bulk Acoustic Wave Resonators, in: 2019 20th International Conference on Solid-State Sensors, Actuators and Microsystems & Eurosensors XXXIII (TRANSDUCERS & EUROSENSORS XXXIII), IEEE, 2019, pp. 1878-1881.

[17] M. Mohammadi, H. Daneshpajooh, M. Hamed, Effect of anisotropy and piezoelectricity on the force-frequency coefficient of AT-cut quartz crystals, *Scientia Iranica*, 23(5) (2016) 2203-2210.

[18] M.M. Mohammadi, M. Hamed, H. Daneshpajooh, High frequency vibrations of quartz crystals subject to initial thermo-mechanical bias, *Scientia Iranica*, 24(2) (2017) 684-697.

[19] M.M. Mohammadi, M. Hamed, Experimental and numerical investigation of force-frequency effect in crystal resonators, *Journal of Vibroengineering*, 18(6) (2016) 3709-3718.

[20] R.D. Mindlin, J. Yang, An introduction to the mathematical theory of vibrations of elastic plates, World Scientific, 2006.

[21] P. Lee, Y. Wang, X. Markenscoff, High-frequency vibrations of crystal plates under initial stresses, *The Journal of the Acoustical Society of America*, 57(1) (1975) 95-105.

[22] M.S. Patel, Nonlinear behavior in quartz resonators and its stability, Rutgers University-Graduate School-New Brunswick, 2008.

Appendix A:

Second-order elastic constants of AT-Cut quartz in Pa [22].

	C_{pq}					
	$q=1$	$q=2$	$q=3$	$q=4$	$q=5$	$q=6$
$p=1$	8.674E+10	-8.261E+09	2.715E+10	-3.655E+09	0.000	0.000
$p=2$	-8.261E+09	1.298E+11	-7.419E+09	5.700E+09	0.000	0.000
$p=3$	2.715E+10	-7.419E+09	1.028E+11	9.921E+09	0.000	0.000
$p=4$	-3.655E+09	5.700E+09	9.921E+09	3.861E+10	0.000	0.000
$p=5$	0.000	0.000	0.000	0.000	6.881E+10	2.534E+09
$p=6$	0.000	0.000	0.000	0.000	2.534E+09	2.901E+10

Third-order elastic constants which were employed in the mathematical model in Pa [22]:

C_{661}	C_{662}	C_{663}	C_{664}
-2.032E+11	2.261E+10	-2.687E+10	8.240E+10

HOW TO CITE THIS ARTICLE

M. M. Mohammadi, M. Hamed, *Force frequency effect in square quartz crystals.*
AUT J. Mech Eng., 5(2) (2021) 215-226.

DOI: [10.22060/ajme.2020.17774.5872](https://doi.org/10.22060/ajme.2020.17774.5872)

